THE JOURNAL OF PHYSICAL CHEMISTRY C

Article

Cite This: J. Phys. Chem. C 2019, 123, 22413−22423

pubs.acs.org/JPCC

Shell Formation Mechanism for Direct Microencapsulation of Nonequilibrium Pure Polyamine Droplet

He Zhang,*[,†,‡] Xin Zhang,[§] Yong Bing Chong,[∥] Junjie Peng,[†] Xinglei Fang,[†] Zhibin Yan,[⊥] Bin Liu,*[,‡] and Jinglei Yang*[,#]

[†]National Engineering Research Center of Novel Equipment for Polymer Processing, Key Laboratory of Polymer Processing Engineering (SCUT), Ministry of Education and [‡]Guangdong Provincial Key Laboratory of Technique and Equipment for Macromolecular Advanced Manufacturing, South China University of Technology, Guangzhou 510641, China

[§]School of Civil and Environmental Engineering and [∥]School of Mechanical and Aerospace Engineering, Nanyang Technological University, 639798 Singapore

[⊥]Guangdong Provincial Key Laboratory of Optical Information Materials and Technology & Institute of Electronic Paper Displays, South China Academy of Advanced Optoelectronics, South China Normal University, Guangzhou 510006, China

[#]Department of Mechanical and Aerospace Engineering, Hong Kong University of Science and Technology, Kowloon, Hong Kong SAR

Supporting Information

ABSTRACT: The understanding of the shell formation mechanism for the novel encapsulation technique via integrating microfluidic T-junction and interfacial polymerization is not only important to fabricate high-quality polyamine microcapsules but also of practical and theoretical significance to the wide application of this method based on nonequilibrium droplets. Herein, using pure polyamine as a targeting core, the shell formation mechanism was investigated by studying the achieved shell structures of the preliminary and final microcapsules and the behavior of nonequilibrium polyamine droplets in the coflow solvent. It reveals the shell has a multilayered structure, i.e., a rough outer layer, a porous middle layer, and a thin but dense inner layer, and the porous middle layer consists of pores with two size levels. This shell structure was correlated to fractal geometry of the polyamine droplet before being encapsulated, which was generated attributed to the interactions between the nonequilibrium polyamine droplet and the coflow solvent, i.e., interdiffusion and spontaneous emulsification. To achieve robust microcapsules, shell thickness and tightness were also studied by varying the composition of the reaction solution in terms of diisocyanate concentration and type of solvent with different polarity. The effect of these two key parameters on shell in this method is very similar to that in the traditional interfacial polymerization. In addition, the influence of the shell-forming stage and shell-growth stage on the robustness of microcapsule was discussed, indicating the former is decisive.

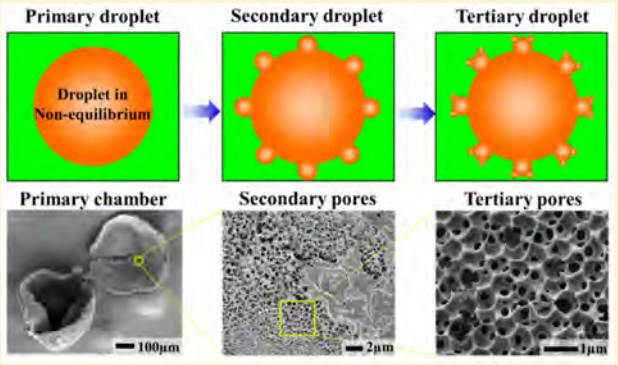

1. INTRODUCTION

Organic polyamine is a class of chemicals which contains two or more amine groups. Attributed to its low cost, broad source, wide variety, and high reactivity, it has been widely used as the monomer to fabricate epoxy, polyurea, nylon, etc. After being encapsulated,[1−9] it can also be adopted in other promising applications, such as self-healing material,[2,6,7,9−14] self-reporting material,[15,16] latent curing agent,[17] pollution absorbent,[18] etc. Among them, self-healing material is the most important and prospective one, owing to the availability of different self-healing chemistries based on polyamine and the high reactivity of polyamine toward many functional groups.[9,19−21]

To date, the encapsulation techniques have been diversified to broaden the range of substances that can be encapsulated for various functional materials.[22−31] However, it is still a challenge for the traditional encapsulation techniques to encapsulate polyamine,[32] attributed to its high reactivity, amphiphilicity, and good solubility in water and most organic solvents. Currently, the explored three main strategies to enwrap polyamines include using hollow microspheres to carry polyamine, encapsulating specially selected polyamines using traditional techniques, and tailoring the physicochemical properties of the core targets containing polyamine for encapsulation.

In the first strategy, any commercial polyamines can be enwrapped theoretically using a two-step process via first

Received: July 10, 2019
Revised: August 23, 2019
Published: August 26, 2019

ACS Publications © 2019 American Chemical Society

DOI: 10.1021/acs.jpcc.9b06544
J. Phys. Chem. C 2019, 123, 22413−22423

Downloaded via HONG KONG UNIV SCIENCE TECHLGY on August 8, 2020 at 12:13:44 (UTC).
See https://pubs.acs.org/sharingguidelines for options on how to legitimately share published articles.

fabricating hollow microcontainers with through-shell channels and then loading the targeting polyamine with/without the aid of vacuum.[2,4,6,11] This strategy is relatively simple and does not involve any chemical reactions during the packaging. However, it is worth noting that the through-shell channels to load polyamine are also the ready channels to release the loaded polyamine, leading to the thermal and long-term instability of the carried polyamine in the fabricated self-healing materials. The second strategy was tried to encapsulate either water-insoluble polyamines using normal emulsion or highly polar polyamines using inverse emulsion. Although some specially selected pure polyamines were attempted to be encapsulated by this way, no successful core−shell structured microcapsules were reported.[1,33] Additionally, even though it works to synthesize microcapsules, this strategy is highly selective to the physiochemical properties of the polyamines for encapsulation, which seriously compromises the application of the achieved microcapsules in self-healing materials. The third strategy by tuning the physicochemical properties of the core targets containing polyamines for encapsulation is widely and deeply investigated in this area, in order to obtain core−shell structured microcapsules containing polyamines. Regulators, such as the good solvents (water,[5,7,14,17] chloroform,[3,10] etc.) and partitioning inhibitors (such as weak acid[8]) for polyamines, were used to minimize the dissolution of polyamines in the continuous phase. Through this strategy, polyamines can be encapsulated using different traditional encapsulation techniques, including inverse Pickering emulsion,[7,17] solvent evaporation,[3,10] and microfluidic.[5,14] Although it can synthesize polyamine microcapsules, it is still strongly selective to the physiochemical properties of the targeting cores and can only deliver microcapsules with low core fraction of polyamine. In most cases, only solution with relatively low concentration (less than 50 wt %) of the highly polar ethylenediamine derivatives, such as diethylenetriamine (DETA),[5,8] triethylenetetramine (TETA),[5,14] tetraethylenepentamine (TEPA),[7,17] etc., can be encapsulated in order to form stable emulsions, which highly restricts their potential applications in self-healing materials.

It can be also seen that the latter two strategies have commonality, that is, how to form stable emulsions before the encapsulation processes. In fact, in the traditional encapsulation techniques using chemical reactions, the formation of a stable emulsion is a prerequisite for a successful encapsulation process for any targeting substances. Since the shell formation mechanisms and the related physicochemical changes during these processes based on stable emulsions are clear and well-studied, the investigations about encapsulating polyamines mainly focus on how to form stable emulsions and to regulate the properties of the synthesized microcapsules. It is worth noting that most of these studies still remain at the stage of exploring and establishing the encapsulation methods/processes for polyamines. It is still challenging to be applied in self-healing materials for the achieved polyamine microcapsules.

Recently, combining the merits of microfluidic in forming and regulating droplets and the flexibility of interfacial polymerization in encapsulation, we directly encapsulated pure polyamine via integrating microfluidic and rapid interfacial polymerization.[9] Since the pure polyamine droplet was encapsulated immediately after its formation, it is in a nonequilibrium status when encapsulated. Our previous investigations have demonstrated the breakthrough by proving the principle, verifying the feasibility of the device, and applying the achieved polyamine microcapsules in a potentially practical self-healing system and a fully autonomously skinlike smart material, respectively.[9,15] However, owing to the nonequilibrium feature of the polyamine droplet, the encapsulation process is completely different from the traditional encapsulation processes based on equilibrium droplets. It involves much more complicate physicochemical changes with multiple phases, multiple compositions, and multiple steps. In addition, the amphiphilicity of polyamine also aggravates the complexity of this encapsulation process. All these lead to the difficulty in understanding the complex shell structure and therefore regulating the physicochemical properties of the achieve microcapsules. Hence, to achieve a more controllable process to fabricate high-quality microcapsules by this method, it is necessary to figure out the shell formation mechanism during the encapsulation process based on nonequilibrium droplets and the influence of interaction between the nonequilibrium polyamine droplet and solvent on the quality of the microcapsules. What is more, this encapsulation technique via integrating microfluidic and rapid interfacial polymerization can not only encapsulate substances that are unable to form stable emulsions but also encapsulate substances that can form stable emulsions.[34] Thus, it is a universal technique to encapsulate a wide variety of substances, which also requires a deeper understanding of the shell formation mechanism for the technique to guide the encapsulation of other substances. In this sense, the investigation of the shell mechanism is of practical and theoretical significance.

2. EXPERIMENTAL SECTION

2.1. Materials. The following chemicals were purchased from Sigma-Aldrich, including tetraethylenepentamine (TEPA), cyclohexane, decalin, *n*-hexadecane, 4,4′-methylenebis(cyclohexyl isocyanate) (HMDI, mixture of isomers), and 1,4-diazabicyclo[2.2.2]octane (DABCO). Microbore polytetrafluoroethylene (PTFE) tubing, T1 with an inner diameter (i.d.) of 0.012 in. and outer diameter (o.d.) of 0.03 in., and T2 with i.d. of 0.022 in. and o.d. of 0.042 in. were purchased from Cole-Parmer. All the chemicals and materials were used as received.

2.2. Encapsulation Process. Microencapsulation of pure polyamine through the integration of microfluidic T-junction and interfacial polymerization was described in our previous study and is schematically shown in Figure 1.[9] Tubing T1 was

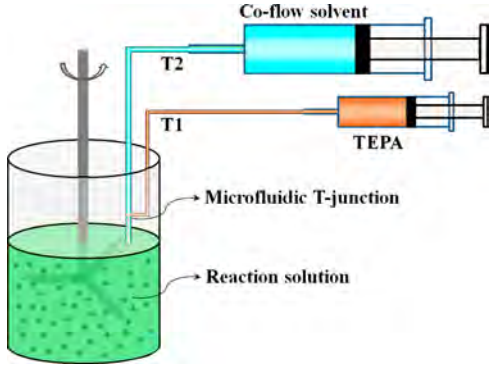

Figure 1. Schematic configuration of the device for encapsulation via integrating microfluidic T-junction and interfacial polymerization.

DOI: 10.1021/acs.jpcc.9b06544
J. Phys. Chem. C 2019, 123, 22413−22423

inserted into tubing T2 to fabricate a T-junction unit (T1/T2). The free end of T1 was connected to a syringe with pure TEPA controlled by a syringe pump (NE1600-Six Syringe Pump), and that of T2 was connected to a syringe with *n*-hexadecane containing 1.0 wt % Arlacel P135 as surfactant controlled by another syringe pump (NE1600-Six Syringe Pump). The reaction solution in a 250 mL beaker was prepared by mixing 1.0 wt % Arlacel P135, 1.0 wt % DABCO, and variable amount (*M*, g) of HMDI into 50.0 mL solvent. The reaction solution was stirred gently at 100−120 rpm using a three-blade propeller driven by mechanical stirring overhead (Caframo, model BDC6015). The beaker was placed in a water bath with temperature controlled by a programmable hot plate (hot plate digital aluminum 230).

Under agitation at room temperature (RT, ∼22−25 °C), TEPA and *n*-hexadecane were fed through the T-junction into the reaction solution with feeding rates of *v* mL/min and 0.5 mL/min, respectively. The feeding process was stopped after the addition of about 12.0 mL of *n*-hexadecane and the corresponding volume of TEPA. This stage was named as the shell-forming stage, and the formed microcapsules at this stage were designated as the preliminary microcapsules. Later on, the mixture was subjected to a shell-growth stage to react at 40 °C for 1 h, 50 °C for 2 h, and 60 °C for 2 h in order. The microcapsules were separated by rinsing the mixture with pure cyclohexane and decanting the supernatant 4−5 times, dried at RT for about 5−10 min, and finally stored in vial with good airtightness.

Table 1 shows the adopted specific parameters for the encapsulation process, including the solvent in the reaction solution for the shell-forming stage, amount of HMDI (*M*, g) in the reaction solution, feeding rate of the pure TEPA (*v*, mL/min), and solvent in the reaction solution for the shell-growth stage. In order to change the solvent in the reaction solution after the shell-forming stage, the preliminary microcapsules were separated from the mixture right after the feeding process and then transferred into another reaction solution consisting of the designated solvent, 6.0 g of HMDI, 1.0 wt % Arlacel P135, and 1.0 wt % DABCO, for further shell growth.

Table 1. Specific Parameters Adopted in This Study[a]

solvent in reaction solution	feeding rate of TEPA (*v*, mL/min)	amount of HMDI (*M*, g)	solvent for shell-growth stage
decalin	0.075	6.0	decalin
decalin	0.05	6.0	decalin
decalin	0.025	6.0	decalin
decalin	0.01	6.0	decalin
decalin	0.005	6.0	decalin
decalin	0.05	2.0	decalin
decalin	0.05	4.0	decalin
decalin	0.05	6.0	decalin
decalin	0.05	8.0	decalin
decalin	0.05	10.0	decalin
decalin	0.05	6.0	decalin
n-hexadecane	0.05	6.0	*n*-hexadecane
decalin	0.05	6.0	*n*-hexadecane
n-hexadecane	0.05	6.0	decalin

[a]Other parameters include the following: polyamine for encapsulation is pure TEPA; coflow solvent is *n*-hexadecane with 1.0 wt % Arlacel P135 as surfactant; reaction solution is 50 mL solvent with 1.0 wt % Arlacel P135 as surfactant, 1.0 wt % DABCO as catalyst, and variable amount of HMDI. Added amount of coflow solvent is about 12.0 mL for each run. After feeding of TEPA, the mixture was subjected to 40 °C for 1 h, 50 °C for 2 h, and 60 °C for 2 h in order.

During one typical process, a high-speed camera (Fastec Imaging with lens Micro-NIKKOR) was adopted to observe the evolution of TEPA droplets at the end of T2.

2.3. Characterization Methods. The morphology, shell structure, size distribution, and shell thickness of microcapsules were characterized using field emission scanning electronic microscopy (FESEM, JEOL JSM-7600F). The averaged diameters with standard deviation (SD) and averaged shell thickness with SD of microcapsules were measured from FESEM images using the software ImageJ. The composition of microcapsules was characterized using thermogravimetric analysis (TGA, AutoTGA Q500). For every test, a sample with the weight of 10.0−30.0 mg was placed in a platinum pan and heated to 600 °C with a ramp rate of 10.0 °C/min under nitrogen atmosphere. The behavior of polyamine droplets with different sizes in the coflow solvent was observed using an optical microscope (Olympus CKX41).

3. RESULTS AND DISCUSSION

3.1. Shell Structure and Formation Mechanism. *3.1.1. Hierarchical Shell Structure of Achieved Polyamine Microcapsule.* Polyurea microcapsules containing pure TEPA were successfully achieved using the proposed device and method through the integration of microfluidic T-junction and interfacial polymerization. Figure 2a shows the general

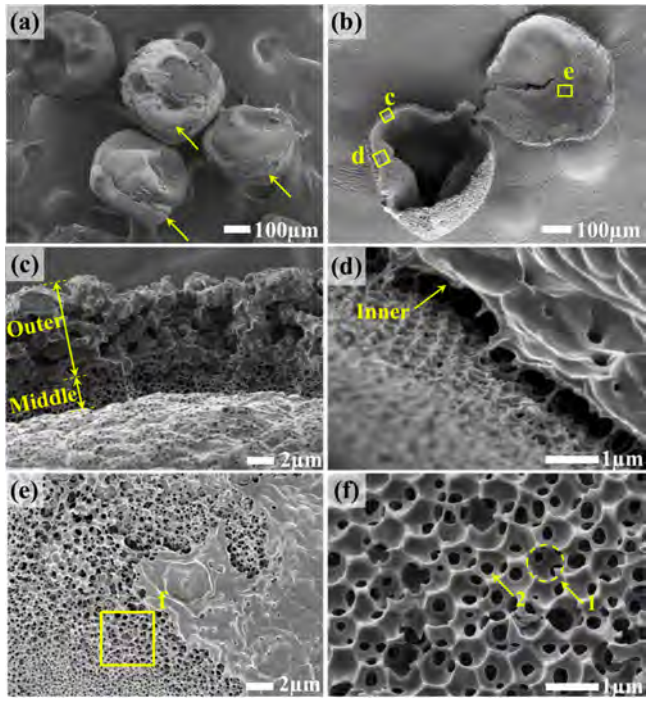

Figure 2. Shell structure of microcapsules containing pure TEPA synthesized through integrating microfluidic T-junction (T1/T2) and interfacial polymerization. (a) General appearance of microcapsules. Arrows indicate formed tails or crowns around microcapsules. (b) Cross section of a fractured typical microcapsule. (c) Enlargement of the cross section showing shell structure along radium. (d) Peeled dense inner wall. (e) Porous structure of the shell after removal of inner wall. (f) Further enlargement of the shell. Arrows 1 and 2 indicate a secondary pore and a tertiary pore, respectively.

DOI: 10.1021/acs.jpcc.9b06544
J. Phys. Chem. C 2019, 123, 22413−22423

appearance of the obtained microcapsules when TEPA was fed at 0.05 mL/min. Tails or crowns with a loose structure were observed for most of the microcapsules, as indicated by the arrows. The cross section of a typical microcapsule is given in Figure 2b, showing that the microcapsule has a perfect core−shell structure. The imaged specimen was prepared by cutting microcapsules and then rinsing and flushing them thoroughly using deionized (DI) water to completely remove the core liquid to eliminate its influence on FESEM imaging. The cross sections zoomed in Figure 2c, d indicate the shell consists of multiple layers with a rough outer layer, a porous middle layer, and a thin but dense inner layer along with the radium inward. As shown in Figure 2d, e, the inner layer could be peeled away when it was flushed heavily by DI water during the sample preparation, revealing that it is weakly connected to the rest of the shell. Further enlargement of the peeled area in Figure 2f shows that there are uniformly distributed small pores with a size smaller than 1 μm (arrow 1 in Figure 2f, denoted as secondary pores). Interestingly, besides the submicrometer pores beneath the inner layer, several pores with a much smaller size (denoted as tertiary pores) were also observed for every secondary pore, as indicated by arrow 2 in Figure 2f.

According to the observations as shown in Figure 2d, f, it is reasonable to assume that the secondary and tertiary pores are hollow spherical structures, which were occupied by some other substances before the sample preparation for FESEM imaging. However, according to the procedure, neither were any gases introduced into the system at the beginning nor were any gases generated during the encapsulation process. Although the reaction between isocyanate and water can generate carbon dioxide,[35] it is unlikely to occur considering the extremely high reactivity between isocyanate and amine in comparison with that between isocyanate and hydroxyl groups at RT and the trace amount of residual water in the system. What is more, the number of pores also eliminates the possibility that they were generated by this reaction. Considering these facts, the substances in the secondary and tertiary pores can only be the polyamine or the solvent or their mixture.

Based on the shell structure of the microcapsule, fractal geometry of the TEPA droplet in *n*-hexadecane before being encapsulated was hypothesized as shown in Figure 3. First, the

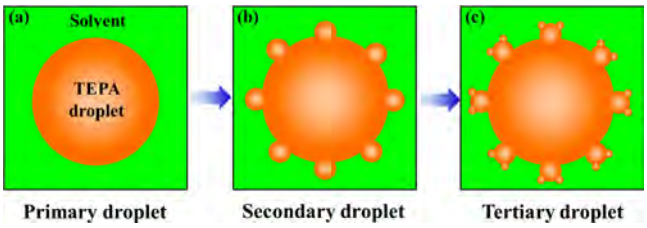

Figure 3. Proposed fractal character of a TEPA droplet in *n*-hexadecane before being encapsulated by interfacial polymerization.

primary polyamine droplet was generated by the T-junction (Figure 3a). However, before getting into the reaction solution for encapsulation, some secondary polyamine droplets appear around the primary droplet (Figure 3b), attributed to some interactions at the interface. Finally, owing to the similar interactions, tertiary polyamine droplets appear around the secondary droplets (Figure 3c). When this kind of structure near the interface between the TEPA droplet and *n*-hexadecane gets into contact with the reaction solution, it is fixed down by the rapid interfacial reaction between polyamine and diisocyanate, forming the observed shell structure for the microcapsules during the encapsulation process. Subsequent sections aim to elucidate the formation mechanism of such a complex structure.

3.1.2. Study on Preliminary Polyamine Microcapsule. Preliminary microcapsules, which form during the shell-forming stage, were collected for characterization using FESEM (Figure 4). As mentioned in our previous study,[9]

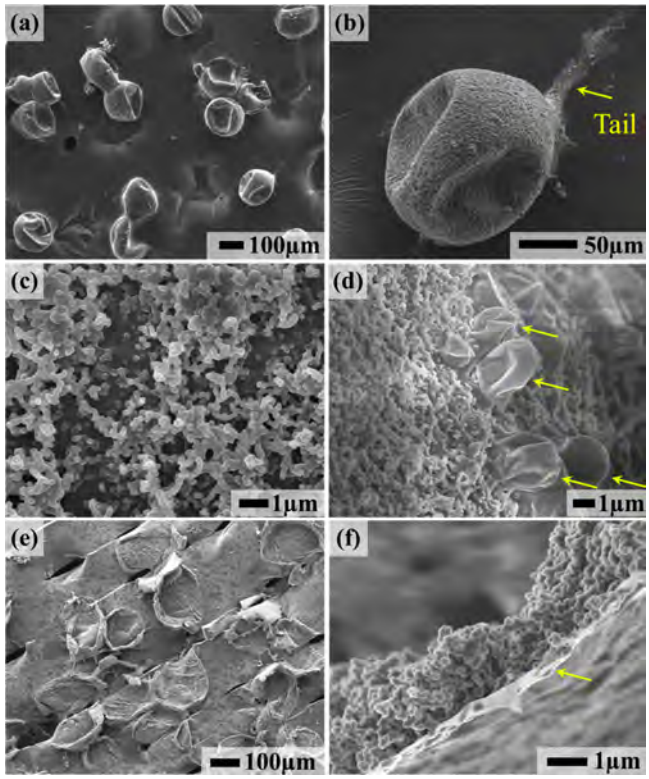

Figure 4. Preliminary microcapsules containing pure TEPA generated right after contact of the mixture from the end of T2 with the reaction solution. (a) General appearance of the preliminary microcapsules. (b) A typical primary microcapsule with a long tail. (c) Deposited polyurea nanoparticles on the shell. (d) Small secondary microcapsules at micrometer scale generated on the shell of the TEPA microcapsule. (e) Collapsed microcapsules after being cut by sharp blade. (f) Cross section showing the dense inner wall, as indicated by the arrow.

these preliminary microcapsules are impermeable so that they are able to keep their spherical shapes under the high vacuum ($<10^{-3}$ Pa) during FESEM imaging (Figure 4a,b), although shrinkage occurs on every preliminary microcapsule. A long tail can also be observed for the preliminary microcapsule, as indicated by the arrow in Figure 3b. Besides the deposited polyurea nanoparticles (Figure 4c), some small microcapsules at micrometer level were also observed on the outer shell of the preliminary microcapsules (arrows in Figure 4d), which may leave the secondary pores in the shell after the removal of core substances. Although the preliminary microcapsules could keep their shapes at high vacuum due to good impermeability, they collapsed immediately when they were cut by a sharp blade (Figure 4e), which means the shells are not rigid enough to keep their spherical shape. Cross section of this preliminary microcapsule was also observed (Figure 4f), showing the

DOI: 10.1021/acs.jpcc.9b06544
J. Phys. Chem. C 2019, 123, 22413−22423

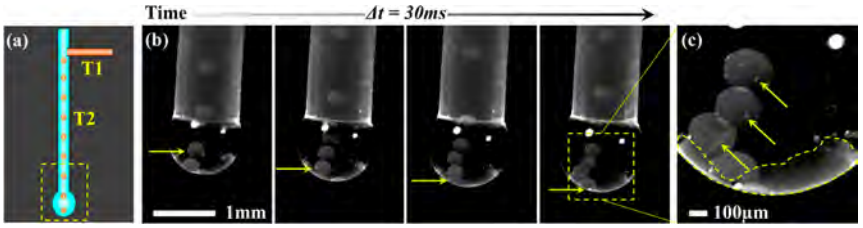

Figure 5. (a) Schematic configuration of T-junction (T1/T2) and the imaged area. (b) Freeze frames with a time interval of 30 ms for neighboring images showing the evolution of the pure TEPA droplet at the end of T2. The four arrows indicate the vanishing of a TEPA droplet. (c) Enlargement showing the generated small secondary droplets on the primary TEPA droplets (as indicated by the arrows and other light dots on the droplets) and the Tyndall effect as indicated by the dashed curve.

deposited polyurea nanoparticles and the dense inner layer, as indicated by the arrow. By comparing the shell structures of the preliminary microcapsules (Figure 4f) and the final microcapsules (Figure 4c), it is indicated that the shell grows outward along the radium direction, which is consistent with that of microcapsule synthesized by interfacial polymerization in traditional water-in-oil emulsions.[36,37]

3.1.3. Behavior of TEPA Droplets in Coflow Solvent. The behavior of TEPA droplet in *n*-hexadecane before flowing into the reaction solution was carefully studied using a high-speed camera. Video S1 shows the behavior of the mixture at the end of T2 (Figure 5a), and Figure 5b shows the freeze frames with a time interval of 30 ms from Video S1 for the evolution of the pure TEPA droplets. It can be seen that the droplet disappeared rapidly sooner after leaving T2, as indicated by the four arrows for a typical TEPA droplet in Figure 5b. In addition, Tyndall effect, i.e. light scattering by particles in a colloid or in a very fine suspension, appeared as illustrated by the opaqueness of *n*-hexadecane at the bottom of the large drop, which could also be observed in every image in Figure 5b and especially in the enlargement in Figure 5c by the dashed curve. This effect implies that the disappearance of the TEPA droplet results from not only the dissolution of TEPA in *n*-hexadecane with a low concentration[8] but also some other interactions that can generate small liquid particles which are able to cause diffuse deflection. Interestingly, enlargement of the TEPA droplet in Figure 5c shows that a number of small bright dots can be observed on every TEPA droplet, as indicated by the arrows and other similar light dots on the surface of TEPA droplets. This kind of structure, i.e., a primary TEPA droplet surrounded by small droplets, is in coincidence with the proposed fractal character as shown in Figure 3. It is reasonable to infer that the particles which cause the Tyndall effect are very small TEPA droplets generated during flowing of the primary TEPA droplet in the coflow solvent.

To further support this phenomenon, more direct evidence for the generation of small droplets around a TEPA droplet in *n*-hexadecane was achieved via dropping the mixture of pure TEPA droplets in *n*-hexadecane from the end of T2 onto a glass slide for observation using an optical microscopy. Video S2 shows the evolution of a TEPA droplet with a diameter of about 550 μm in *n*-hexadecane right after its generation. In the beginning, the TEPA droplet stayed stable in *n*-hexadecane for a short while. Shortly afterward, many small droplets at micrometer scale suddenly appeared around the droplet and flowed away, as shown in a typical freeze frame in Figure 6a. Finally, the primary TEPA droplet collapsed, leaving a huge number of small TEPA droplets (Video S2). These phenomena are quite similar to those observed by the high-speed camera, regarding the disappearance of the droplet and

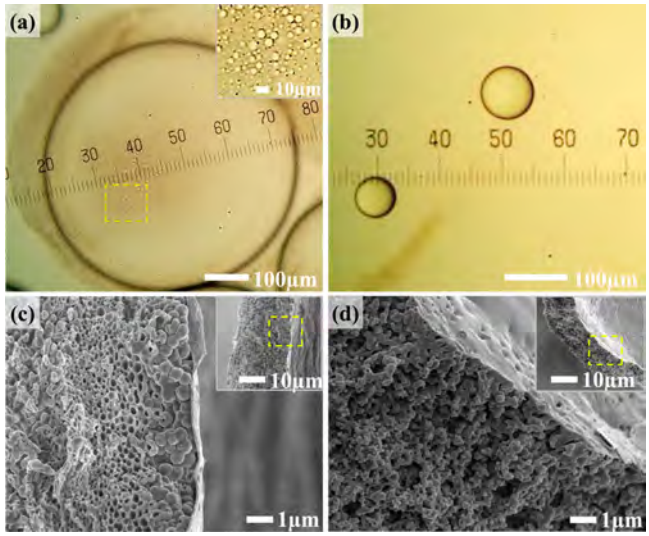

Figure 6. (a) Optical microscopic image showing generation of small secondary droplets near the interface of TEPA and *n*-hexadecane. (b) Behavior of small TEPA droplets in *n*-hexadecane without generation of visible small secondary droplets. (c) Shell with middle porous layer of a large microcapsule (about 450 μm). (d) Shell with less pores of a small microcapsule (about 100 μm).

generation of a large number of smaller droplets to cause the Tyndall effect. However, a different phenomenon was observed for a smaller TEPA droplet with a diameter about 85 μm in *n*-hexadecane, as shown in Video S3 and Figure 6b for a typical freeze frame. At a time scale comparable to that for the large TEPA droplet, this small droplet was much more stable, and no visible small droplets could be observed around it. The difference in behavior caused by the droplet size was correlated to the shell structure of the synthesized microcapsules with similar sizes. Figure 6c, d show the cross sections of a large microcapsule (about 450 μm) and a small microcapsule (about 100 μm), respectively. An evident porous layer could be observed in the shell of the large microcapsule, whereas no visible pores could be seen for the smaller one, which is consistent with the phenomena observed for the TEPA droplets with similar sizes.

3.1.4. Proposed Shell Formation Mechanism. Borrowing the idea about spontaneous emulsification of oil drops in water by Rang and Miller,[38] we proposed herein a mechanism to illustrate the behavior of TEPA droplet before getting into the reaction solution, as schematically demonstrated in Figure 7. Upon the generation of a nonequilibrium primary TEPA droplet in *n*-hexadecane with surfactant Arlacel P135, interdiffusion of TEPA molecules and *n*-hexadecane takes

DOI: 10.1021/acs.jpcc.9b06544
J. Phys. Chem. C 2019, 123, 22413−22423

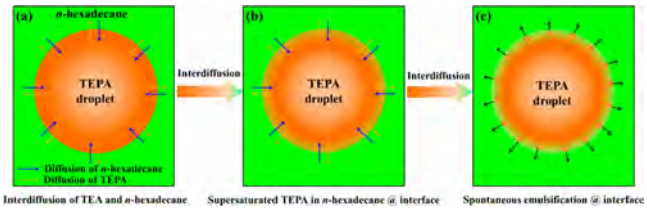

Figure 7. Mechanism for spontaneous emulsification of TEPA in *n*-hexadecane. (a) Primary TEPA droplet in *n*-hexadecane right after generation. (b) Formation of a supersaturated solution of TEPA in *n*-hexadecane due to interdiffusion of TEPA molecules and *n*-hexadecane near the interface. (c) Generation of small TEPA droplets at micrometer scale at the interface due to spontaneous emulsification.

place immediately due to their mutual solubility in each other although it is relatively low (Figure 7a).[8] With the progress of the interdiffusion process, mixture near the interface turns to supersaturated TEPA solution in the diffused *n*-hexadecane (Figure 7b). Owing to the low interfacial tension between TEPA and *n*-hexadecane with the presence of surfactant Arlacel P135, polyamine near the interface nucleates and grows to small droplets at micrometer scale, leading to the spontaneous emulsification of TEPA in *n*-hexadecane (Figure 7c). Finally, the generated small droplets, as the secondary TEPA droplets, leave the interface with *n*-hexadecane (Figure 6a). Similarly, attributed to the same mechanism, tertiary tiny TEPA droplets grow around the secondary TEPA droplets during the process, resulting in the formation of fractal geometry.

Upon flowing of a TEPA droplet with this kind of structure into the reaction solution, the dissolved TEPA in *n*-hexadecane reacts instantly with the diisocyanate, i.e., HMDI, forming the microcapsule tail. As for the generated secondary droplets at micrometer scale on the primary TEPA droplet, they are fixed on the surface of the droplet and appear as the secondary microcapsules, as shown in Figure 4d. If the leaving secondary droplets with a relatively short distance from the surface are trapped by the formed polyurea network around the primary droplet, they remain on the surface of the preliminary microcapsule and appear as the porous middle layer of the shell after the removal of core liquid during sample preparation. When the preliminary microcapsules with this kind of structure were subjected to elevated temperatures for certain duration, the shell was thickened by forming the rough outer layer through rapid interfacial polymerization between the diffused polyamine and diisocyanate.

According to the mechanism, interdiffusion between TEPA and *n*-hexadecane near the interface is a prerequisite for the spontaneous emulsification process. Although the solubility is low, TEPA can still dissolve in *n*-hexadecane, which was proved by Lu et al.[8] when they measured the solubility of an analogue, i.e., triethylenetetramine (TETA), in *n*-hexadecane. The phase-separated TEPA from a mixture of TEPA and *n*-hexadecane/decalin after thorough mixing and phase separation was collected and characterized using TGA (Figure 8), revealing that both *n*-hexadecane and decalin can dissolve in TEPA and that decalin has a higher solubility. Given the fact that the interdiffusion takes time, it is reasonable that the spontaneous emulsification and the generation of small TEPA droplets can only occur after a short period for the primary TEPA droplet in *n*-hexadecane (Video S2). The reason why no or less visible small droplets could be observed for smaller

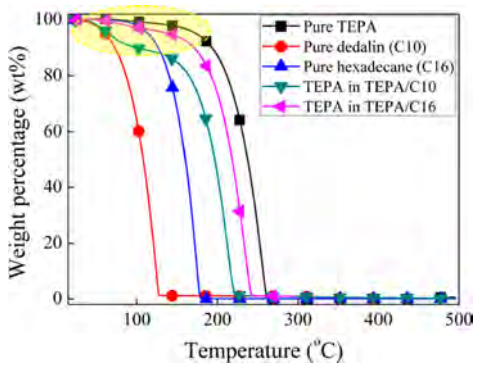

Figure 8. TGA curves of pure TEPA, pure decalin, pure *n*-hexadecane, phase-separated TEPA from a mixture of TEPA/decalin, and phase-separated TEPA from a mixture of TEPA/*n*-hexadecane.

TEPA droplet can also be explained by this model, according to Laplace's equation shown as follows

$$\Delta P = \frac{2\gamma}{r} \quad (1)$$

where ΔP means the extra pressure exerted to the TEPA droplet due to the curvature of the droplet, γ is the interfacial tension, and r is the radius of the droplet. Based on this equation, the smaller the droplet, the higher the exerted extra pressure on the droplet. Consequently, the interdiffusion and therefore the spontaneous emulsification are more difficult. The decrease of interdiffusion was indirectly demonstrated by the fewer tails or crowns, formed by the reaction of the dissolved TEPA with diisocyanate in the solvent, on the smaller microcapsules. Figure 9 shows the morphology of the

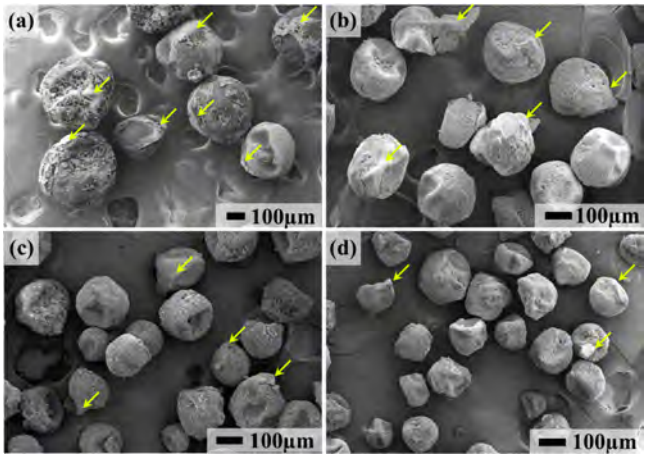

Figure 9. Tails or crowns on microcapsules, owing to the dissolved small amount of TEPA in *n*-hexadecane, with respect to the size of microcapsule. Feeding rate of TEPA for (a) 0.05, (b) 0.025, (c) 0.01, and (d) 0.005 mL/min.

obtained microcapsules with respect to the feeding rate of TEPA when the feeding rate of *n*-hexadecane was fixed at 0.5 mL/min. As indicated by the arrows, the attached tails or crowns on the microcapsules decrease with decreasing the microcapsule size.

3.2. Regulation of Shell Thickness and Tightness.

Besides the shell structure, the shell thickness and tightness of the synthesized microcapsule were also investigated. For self-healing applications, microcapsules with a highly impermeable

DOI: 10.1021/acs.jpcc.9b06544
J. Phys. Chem. C 2019, 123, 22413−22423

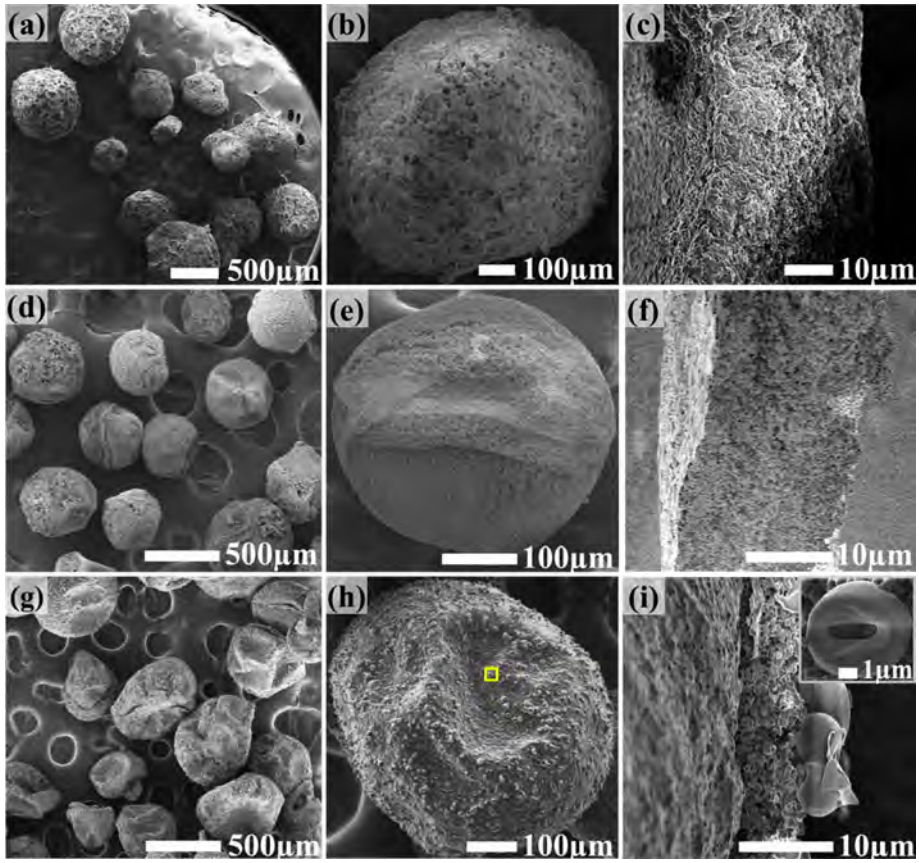

Figure 10. Influence of HMDI concentration in the reaction solution on the structure, cross section, and morphology of the obtained microcapsules containing pure TEPA. (a–c) 2.0 g of HMDI, (d–f) 6.0 g of HMDI, and (g–i) 10.0 g of HMDI. Feeding rates for TEPA and coflow solvent were 0.05 and 0.5 mL/min, respectively.

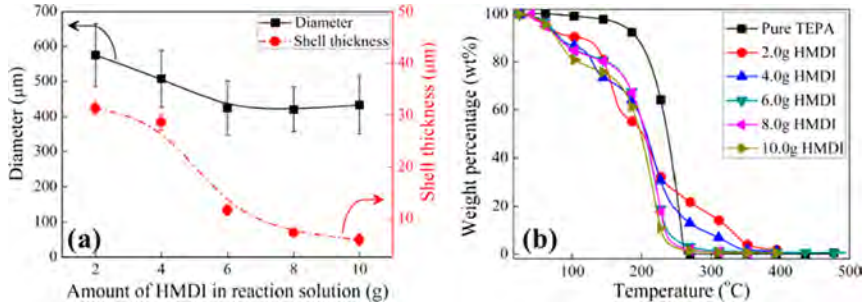

Figure 11. (a) Trends of diameter and shell thickness with respect to the adopted amount of HMDI in reaction solution and (b) TGA curves showing the influence of the adopted amount of HMDI in the reaction solution on the composition of the obtained microcapsules containing pure TEPA.

shell are usually more desirable to retain the encapsulated core for in situ healing upon mechanical damages. However, for the microcapsules synthesized using interfacial polymerization, a too impermeable shell, especially at the early stage, affects adversely the quality of the final microcapsules, as the shell growth highly depends on the diffusion of substance through the formed wall at the early stage. Hence, this section aims to discuss the effect of the two key parameters in the reaction solution, i.e., the HMDI concentration and the type of solvent in the reaction solution, on the shell thickness and tightness of the final microcapsules.

3.2.1. Influence of HMDI Concentration in Reaction Solution. Different amounts of HMDI, from 2.0 to 10.0 g, were adopted for the encapsulation process using the same procedure (Table 1). Figures 10 and 11 show the morphology, cross section, and composition of the obtained microcapsules, respectively. Dry irregular microcapsules (Figure 10a) with low core fraction of TEPA (Figure 11b) could be obtained when 2.0 g of HMDI was used. Although dry microcapsules for processes with 8.0 and 10.0 g of HMDI could be obtained and no microcapsules fractured during the drying process (Figure 12a), they turn wet and stick to each other during their storage in sealed vials (Figure 12b). It is observed in Figures 10b, e, h, and 11a that with increasing the amount of HMDI in the reaction solution, the debris on microcapsules and the size of microcapsules decrease. Microcapsules from processes with 2.0 g of HMDI are completely covered with loose structure while those from the process with 10.0 g of HMDI are not. In stark

DOI: 10.1021/acs.jpcc.9b06544
J. Phys. Chem. C 2019, 123, 22413–22423

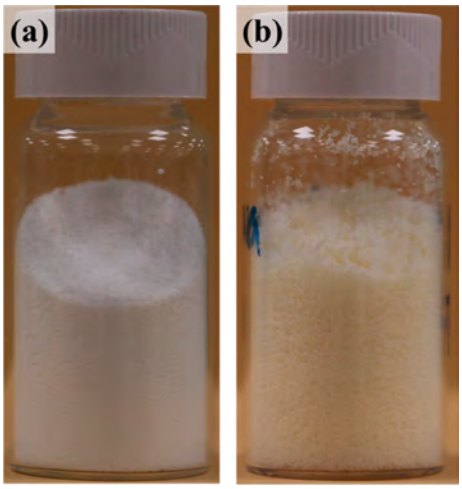

Figure 12. Final appearance of microcapsules obtained when (a) 6.0 g of HMDI was used in the reaction solution and (b) 10.0 g of HMDI was used in the reaction solution.

contrast, fractured small secondary microcapsules could be observed outside the microcapsules for the batch with 10.0 g of HMDI (Figure 10h, i). Meanwhile, the shell thickness decreases with increasing HMDI from 2.0 to 10.0 g (Figure 11a). From this observation, it can be seen that the process with 6.0 g of HMDI produced the best microcapsules, which are flow-free without leakage (Figure 12a) and possess a suitable shell thickness (Figure 11a) and high core content (Figure 11b). This trend indicates that the HMDI concentration in the reaction solution plays a key role to control the shell thickness and tightness of the microcapsule in the encapsulation process.

A model was proposed to explain the influence of HMDI concentration on the achieved microcapsules (Figure 13). When the HMDI concentration is low, the TEPA molecules diffused across the interface into the reaction solution have to diffuse for a longer distance to find enough HMDI molecules for reaction, as shown in Figure 13a. In this case, the shell will be thicker and looser, and thus the microcapsules will be larger. Attributed to the looser structure and less amount of HMDI available for reaction, more TEPA molecules diffuse through the shell into the reaction solution, leading to the lower amount of TEPA encapsulated in the final microcapsules, as indicated by the TGA curves in Figure 11b. Although less HMDI in the reaction solution consumes less polyamine seemingly, it is necessary to keep in mind that the added amount of HMDI in the reaction solution far exceeds the required amount for shell formation, which is the strategy to solidify the diffused polyamine to form the shell. Owing to the more diffused polyamine and looser structure of the shell, the solvent in the reaction solution can diffuse into the microcapsule more easily, resulting in the higher fraction of solvent in the final microcapsules.

However, a too high concentration of HMDI in the reaction solution is also detrimental to the encapsulation process. Figure 13b schematically shows the situation for an encapsulation process with a higher HMDI concentration. Attributed to the abundant HMDI near the interface, the diffused TEPA molecules can react with them in a much shorter distance to form a thinner but denser wall, which makes further diffusion of TEPA molecules more difficult to form a thicker shell. Consequently, only a thin outer rough layer can form to protect the small secondary microcapsules on the primary microcapsule, leaving them naked outside and vulnerable to be broken during their storage. Notably, although the microcapsules turned wet because of the released liquid from the fractured secondary microcapsules, the majority of the liquid is still tightly sealed in the primary chamber, owing to the good impermeability of the thin inner layer. Hence, an optimum concentration of shell-forming monomer in the reaction solution is crucial to produce microcapsules with optimum shell thickness and tightness. In the case of encapsulating pure TEPA herein, the optimum concentration of HMDI is around 6.0 g, which can eliminate the undesirable loose and thin shell respectively due to the lower and higher concentration of HDMI.

3.2.2. Influence of Solvent in Reaction Solution. Besides the HMDI concentration, the solvent in the reaction solution also influences the encapsulation process. The previously mentioned model in Figure 7 for the formation of fractal geometry only describes the influence of interactions between coflow solvent and polyamine on the formed shell structure. How the solvent in the reaction solution affects the shell structure is unable to be achieved directly due to the complicate physicochemical process upon the flowing of coflow solvent and polyamine droplets into the reaction solution. Because of this, the influence of solvent in the reaction solution was studied comparatively. In an encapsulation process, *n*-hexadecane was used to replace decalin in the reaction solution. Similar to microcapsules obtained from the process with 10.0 g of HMDI, the collected microcapsules were

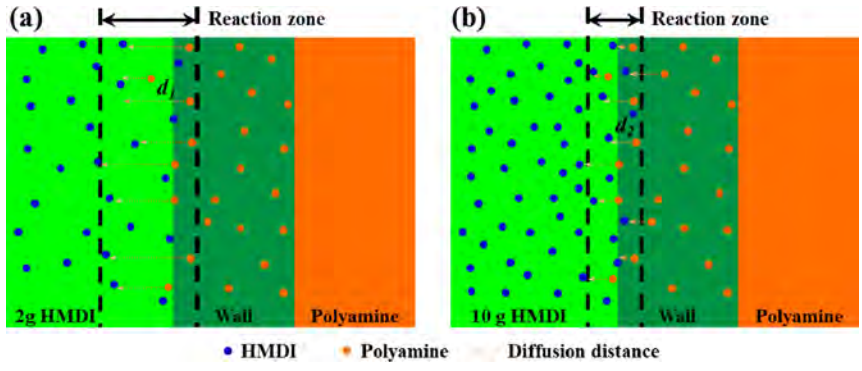

Figure 13. Proposed model explaining influence of HMDI concentration on shell thickness and tightness. (a) Diffusion distance at a relatively lower concentration of HMDI, i.e.. 2.0 g, and (b) diffusion distance at a relatively higher concentration of HMDI, i.e., 10.0 g.

DOI: 10.1021/acs.jpcc.9b06544
J. Phys. Chem. C 2019, 123, 22413−22423

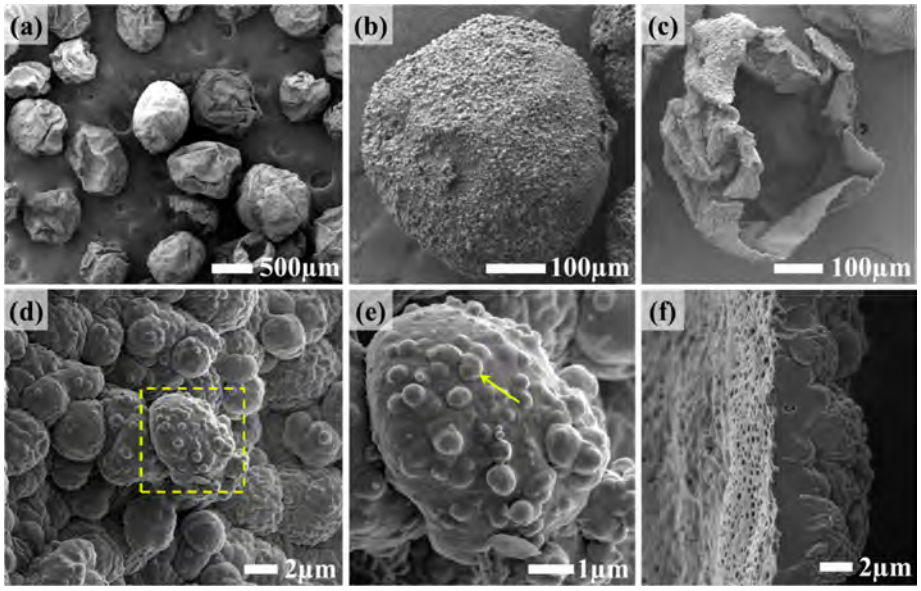

Figure 14. Morphology and structure of microcapsules containing pure TEPA obtained when *n*-hexadecane was used as the solvent for the reaction solution. (a) General appearance with shrinkage. (b) A typical microcapsule. (c) A fractured microcapsule showing core−shell structure. (d) Surface morphology showing the secondary microsphere. (e) Enlargement from (d) showing the tertiary microspheres and (f) cross section showing dense inner shell with larger thickness.

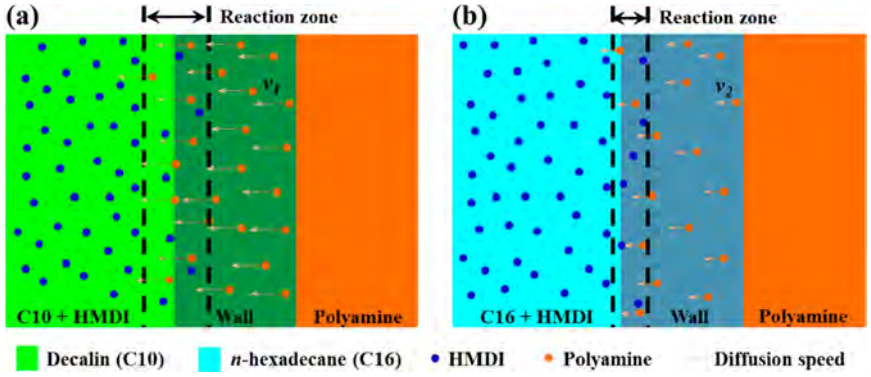

Figure 15. Influence of solvent in the reaction solution on the shell formation during microencapsulation: (a) decalin (C10) and (b) *n*-hexadecane (C16). Decalin has relatively higher polarity compared to *n*-hexadecane and thus has higher solubility to polyamine and swellability to the formed polyurea wall.

dry and flow-free right after collection but turned wet and sticky during their storage in a sealed vial. Figure 14 shows FESEM images of the obtained TEPA microcapsules when *n*-hexadecane was used as the solvent in the reaction solution. The microscopic morphology and structure of the microcapsules also revealed the similarity to that of microcapsules obtained from process with 10.0 g of HMDI, in terms of shrunk shell (Figure 14a), relatively smoother surface (Figure 14b), naked secondary microspheres (Figure 14b, d), and thinner shell (Figure 14f). Different from the microcapsules obtained from the process using the reaction solution with 6.0 g of HMDI and decalin (Figure 2c), the microcapsule herein does not have the multilayered structure, but only the relatively thicker dense section (Figure 14f). It suggests that the solvent in the reaction solution indeed affects the spontaneous emulsification of TEPA droplet. Since the polarity of *n*-hexadecane is lower than that of decalin, the interdiffusion between TEPA and *n*-hexadecane is slower and less than that between TEPA and decalin, as demonstrated by the TGA curves in Figure 8. Consequently, the spontaneous emulsification is also slower, resulting in the less generated smaller TEPA droplets and therefore fewer pores in the cross section.

Another impact of the lower solubility of TEPA in *n*-hexadecane is that it is more difficult for the diffusion of TEPA across the interface or the formed wall. A model in Figure 15 was proposed to illuminate this difference. Due to the relatively lower polarity, *n*-hexadecane has a lower ability to swell the formed polyurea shell compared to decalin. Therefore, the dissolved amount and diffusion speed of TEPA decrease when *n*-hexadecane was adopted. As a consequence of this, the region for the reaction between TEPA and HMDI is closer to the interface, leading to the thinner but denser shell, as schematically shown in Figure 15b. The dense shell, in turn, slows down the further diffusion of TEPA for reaction to thicken it. Since shell formed at the early stage is not covered by the later grown rough outer wall, a detailed feature about the fractal geometry was solidified and reserved for this microcapsule, as shown in Figure 14d for the secondary structure and Figure 14e for the tertiary structure. This

DOI: 10.1021/acs.jpcc.9b06544
J. Phys. Chem. C 2019, 123, 22413−22423

observation directly supports the mechanism proposed previously.

In order to clarify which stage, i.e., the shell-forming stage to form the preliminary microcapsule or the shell-growth stage to achieve the final microcapsule, has a higher influence on the quality of the synthesized microcapsules, other two control experiments were conducted by changing the solvent in the reaction solution for the shell-growth stage (Table 1). In one control, the obtained preliminary microcapsules in a reaction solution with decalin as the solvent were separated and transferred into a reaction solution with *n*-hexadecane as the solvent for the shell-growth stage. After the same reaction procedure at elevated temperatures, dry microcapsules could be achieved successfully by this process, although they shrink more and have a thinner shell (Figure 16). In another control,

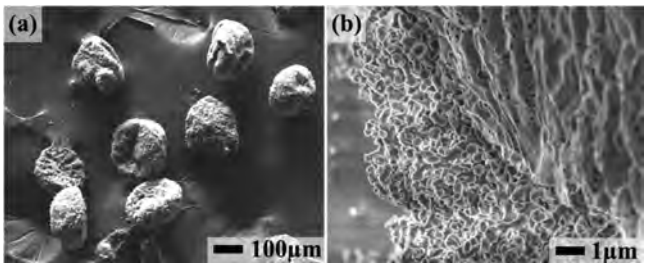

Figure 16. (a) Appearance and (b) shell structure of TEPA microcapsules obtained from the process using decalin as the solvent for the shell-forming stage and *n*-hexadecane as the solvent for the shell-growth stage.

the obtained preliminary microcapsules in a reaction solution with *n*-hexadecane as the solvent were separated and transferred into a reaction solution with decalin as the solvent. However, the collected microcapsules behaved the same as those obtained from the process using *n*-hexadecane as the solvent for both shell-forming and shell-growth stages. These comparisons indicate that the shell-forming stage has a higher influence than the shell-growth stage toward the final properties of the synthesized microcapsules.

Through the experiments and observations, it can be concluded that the shell growth in this encapsulation process is very similar to that in the encapsulation process using interfacial polymerization in traditional emulsions.[39] The shell thickness and tightness of the final microcapsules are largely influenced by the swelling power of the suspension mixture, via controlling the shell permeability and therefore the diffusion of monomers for shell formation.

4. CONCLUSIONS

Using pure polyamine as the targeting core, this investigation shed light on the shell structure, thickness, and tightness of microcapsules synthesized through integrating microfluidic T-junction and interfacial polymerization. The mechanism for shell formation by this innovative method was carefully studied by observing the microscopic shell structures of the preliminary and final microcapsules and behavior of polyamine droplet in the coflow solvent. It is observed that the shell has multiple layers, i.e., a rough outer layer, a porous middle layer, and a thin but dense inner layer, and the porous middle layer consists of pores with two size levels. Fractal structure of the polyamine droplet before getting into the reaction solution was proposed and was explained by interactions between the nonequilibrium polyamine droplet and coflow solvent, i.e., interdiffusion and spontaneous emulsification. The shell thickness and tightness have mutual influence on each other and are determined by the HMDI concentration and the solvent in the reaction solution. HMDI with a moderate concentration and a solvent with relatively higher polarity are beneficial to forming a robust shell for the synthesized microcapsules. It is found that the shell-forming stage has a higher influence on the quality of the final microcapsules than the shell-growth stage. This investigation has a practical and theoretical significance to apply the encapsulation method through integrating microfluidic and interfacial polymerization, considering the broad applications of the synthesized polyamine microcapsules and the versatility of this method for a wide variety of functional substances.

■ ASSOCIATED CONTENT

Supporting Information

The Supporting Information is available free of charge on the ACS Publications website at DOI: 10.1021/acs.jpcc.9b06544.

Behavior of TEPA droplet in *n*-hexadecane at the end of T2 (AVI)

Evolution of a TEPA droplet with a diameter of about 550 μm in *n*-hexadecane right after its generation (MP4)

Behavior of a TEPA droplet with a diameter about 85 μm in *n*-hexadecane (MP4)

■ AUTHOR INFORMATION

Corresponding Authors

*E-mail: zhanghe@scut.edu.cn (H.Z.).
*E-mail: bliu@scut.edu.cn (B.L.).
*E-mail: maeyang@ust.hk (J.Y.).

ORCID

He Zhang: 0000-0001-7864-0305
Yong Bing Chong: 0000-0003-1681-0246
Jinglei Yang: 0000-0002-9413-9016

Notes

The authors declare no competing financial interest.

■ ACKNOWLEDGMENTS

We thank the SUG from HKUST (R9365), Hong Kong Research Grants Council (Project No. N_HKUST631/18), the National Natural Science Foundation of China (Grand No. 51903090), the Natural Science Foundation of Guangdong Province (Grant No. 2016A030313486, 2017A030313270, and 2018A030313264), and the Science and Technology Planning Project of Guangdong Province (Grant No. 2017B090901038) for financial support.

■ REFERENCES

(1) McIlroy, D. A.; Blaiszik, B. J.; Caruso, M. M.; White, S. R.; Moore, J. S.; Sottos, N. R. Microencapsulation of a Reactive Liquid-Phase Amine for Self-Healing Epoxy Composites. *Macromolecules* **2010**, *43*, 1855−1859.

(2) Jin, H.; Mangun, C. L.; Stradley, D. S.; Moore, J. S.; Sottos, N. R.; White, S. R. Self-Healing Thermoset using Encapsulated Epoxy-Amine Healing Chemistry. *Polymer* **2012**, *53*, 581−587.

(3) Li, Q.; Mishra, A. K.; Kim, N. H.; Kuila, T.; Lau, K.-t.; Lee, J. H. Effects of Processing Conditions of Poly(methylmethacrylate) Encapsulated Liquid Curing Agent on the Properties of Self-Healing Composites. *Composites, Part B* **2013**, *49*, 6−15.

DOI: 10.1021/acs.jpcc.9b06544
J. Phys. Chem. C 2019, 123, 22413−22423

(4) Zhang, H.; Yang, J. Etched Glass Bubbles as Robust Micro-Containers for Self-Healing Materials. *J. Mater. Chem. A* **2013**, *1*, 12715−12720.
(5) Chen, P. W.; Cadisch, G.; Studart, A. R. Encapsulation of Aliphatic Amines Using Microfluidics. *Langmuir* **2014**, *30*, 2346−2350.
(6) Jin, H. H.; Mangun, C. L.; Griffin, A. S.; Moore, J. S.; Sottos, N. R.; White, S. R. Thermally Stable Autonomic Healing in Epoxy using a Dual-Microcapsule System. *Adv. Mater.* **2014**, *26*, 282−287.
(7) Yi, H.; Deng, Y. H.; Wang, C. Y. Pickering Emulsion-Based Fabrication of Epoxy and Amine Microcapsules for Dual Core Self-Healing Coating. *Compos. Sci. Technol.* **2016**, *133*, 51−59.
(8) Lu, X.; Katz, J. S.; Schmitt, A. K.; Moore, J. S. A Robust Oil-in-Oil Emulsion for the Nonaqueous Encapsulation of Hydrophilic Payloads. *J. Am. Chem. Soc.* **2018**, *140*, 3619−3625.
(9) Zhang, H.; Zhang, X.; Bao, C.; Li, X.; Sun, D.; Duan, F.; Friedrich, K.; Yang, J. Direct Microencapsulation of Pure Polyamine by Integrating Microfluidic Emulsion and Interfacial Polymerization for Practical Self-Healing Materials. *J. Mater. Chem. A* **2018**, *6*, 24092−24099.
(10) Li, Q.; Siddaramaiah; Kim, N. H.; Hui, D.; Lee, J. H. Effects of Dual Component Microcapsules of Resin and Curing Agent on the Self-Healing Efficiency of Epoxy. *Composites, Part B* **2013**, *55*, 79−85.
(11) Zhang, H.; Wang, P.; Yang, J. Self-Healing Epoxy via Epoxy−Amine Chemistry in Dual Hollow Glass Bubbles. *Compos. Sci. Technol.* **2014**, *94* (0), 23−29.
(12) Zhang, H.; Yang, J. Development of Self-Healing Polymers via Amine−Epoxy Ehemistry: I. Properties of Healing Agent Carriers and the Modelling of a Two-Part Self-Healing System. *Smart Mater. Struct.* **2014**, *23*, 065003.
(13) Zhang, H.; Yang, J. Development of Self-Healing Polymers via Amine−Epoxy Ehemistry: II. Systematic Evaluation of Self-Healing Performance. *Smart Mater. Struct.* **2014**, *23*, 065004.
(14) Neuser, S.; Chen, P. W.; Studart, A. R.; Michaud, V. Fracture Toughness Healing in Epoxy Containing Both Epoxy and Amine Loaded Capsules. *Adv. Eng. Mater.* **2014**, *16*, 581−587.
(15) Zhang, H.; Zhang, X.; Bao, C.; Li, X.; Duan, F.; Friedrich, K.; Yang, J. Skin-Inspired, Fully Autonomous Self-Warning and Self-Repairing Polymeric Material under Damaging Events. *Chem. Mater.* **2019**, *31*, 2611−2618.
(16) Li, W.; Matthews, C. C.; Yang, K.; Odarczenko, M. T.; White, S. R.; Sottos, N. R. Damage Detection: Autonomous Indication of Mechanical Damage in Polymeric Coatings. *Adv. Mater.* **2016**, *28*, 2275−2275.
(17) Li, J.; Hughes, A. D.; Kalantar, T. H.; Drake, I. J.; Tucker, C. J.; Moore, J. S. Pickering-Emulsion-Templated Encapsulation of a Hydrophilic Amine and Its Enhanced Stability Using Poly(allyl amine). *ACS Macro Lett.* **2014**, *3*, 976−980.
(18) Puxty, G.; Rowland, R.; Allport, A.; Yang, Q.; Bown, M.; Burns, R.; Maeder, M.; Attalla, M. Carbon Dioxide Postcombustion Capture: A Novel Screening Study of the Carbon Dioxide Absorption Performance of 76 Amines. *Environ. Sci. Technol.* **2009**, *43*, 6427−6433.
(19) Billiet, S.; Van Camp, W.; Hillewaere, X. K. D.; Rahier, H.; Du Prez, F. E. Development of Optimized Autonomous Self-Healing Systems for Epoxy Materials Based on Maleimide Chemistry. *Polymer* **2012**, *53*, 2320−2326.
(20) Lei, H.; Wang, S.; Liaw, D. J.; Cheng, Y.; Yang, X.; Tan, J.; Chen, X.; Gu, J.; Zhang, Y. Tunable and Processable Shape-Memory Materials Based on Solvent-Free, Catalyst-Free Polycondensation between Formaldehyde and Diamine at Room Temperature. *ACS Macro Lett.* **2019**, 582−587.
(21) Wicks, D. A.; Yeske, P. E. Amine Chemistries for Isocyanate-Based Coatings. *Prog. Org. Coat.* **1997**, *30*, 265−270.
(22) Benita, S. *Microencapsulation: Methods and Industrial Applications*, second ed.; CRC Press: Boca Raton, FL, 2005.
(23) Sun, D.; Zhang, H.; Zhang, X.; Yang, J. Robust Metallic Microcapsules: A Direct Path to New Multifunctional Materials. *ACS Appl. Mater. Interfaces* **2019**, *11*, 9621−9628.
(24) Cao, S. S.; Tang, R.; Sudlow, G.; Wang, Z. Y.; Liu, K. K.; Luan, J. Y.; Tadepalli, S.; Seth, A.; Achilefu, S.; Singamaneni, S. Shape-Dependent Biodistribution of Biocompatible Silk Microcapsules. *ACS Appl. Mater. Interfaces* **2019**, *11*, 5499−5508.
(25) Chong, Y.-B.; Zhang, H.; Yue, C. Y.; Yang, J. Fabrication and Release Behavior of Microcapsules with Double-Layered Shell Containing Clove Oil for Antibacterial Applications. *ACS Appl. Mater. Interfaces* **2018**, *10*, 15532−15541.
(26) Elbadawi, C.; Queralt, R. T.; Xu, Z. Q.; Bishop, J.; Ahmed, T.; Kuriakose, S.; Walia, S.; Toth, M.; Aharonovich, I.; Lobo, C. J. Encapsulation-Free Stabilization of Few-Layer Black Phosphorus. *ACS Appl. Mater. Interfaces* **2018**, *10*, 24327−24331.
(27) Hong, C. S.; Park, J. H.; Lee, S.; Rhoo, K. Y.; Lee, J. T.; Paik, S. R. Fabrication of Protease-Sensitive and Light-Responsive Microcapsules Encompassed with Single Layer of Gold Nanoparticles by Using Self-Assembly Protein of alpha-Synuclein. *ACS Appl. Mater. Interfaces* **2018**, *10*, 26628−26640.
(28) Lin, P. C.; Yan, Q.; Wei, Z.; Chen, Y.; Chen, S. Q.; Wang, H. Y.; Huang, Z. R.; Wang, X. Z.; Cheng, Z. D. Chiral Photonic Crystalline Microcapsules with Strict Monodispersity, Ultrahigh Thermal Stability, and Reversible Response. *ACS Appl. Mater. Interfaces* **2018**, *10*, 18289−18299.
(29) Luo, Q. M.; Wang, Y. F.; Chen, Z. H.; Wei, P. R.; Yoo, E.; Pentzer, E. Pickering Emulsion-Templated Encapsulation of Ionic Liquids for Contaminant Removal. *ACS Appl. Mater. Interfaces* **2019**, *11*, 9612−9620.
(30) Odrobinska, J.; Gumieniczek-Chlopek, E.; Szuwarzynski, M.; Radziszewska, A.; Fiejdasz, S.; Straczek, T.; Kapusta, C.; Zapotoczny, S. Magnetically Navigated Core-Shell Polymer Capsules as Nanoreactors Loadable at the Oil/Water Interface. *ACS Appl. Mater. Interfaces* **2019**, *11*, 10905−10913.
(31) Zou, Y.; Song, J.; You, X.; Yao, J.; Xie, S.; Jin, M.; Wang, X.; Yan, Z.; Zhou, G.; Shui, L. Interfacial Complexation Induced Controllable Fabrication of Stable Polyelectrolyte Microcapsules using All-Aqueous Droplet Microfluidics for Enzyme Release. *ACS Appl. Mater. Interfaces* **2019**, *11*, 21227−21238.
(32) Zhu, D. Y.; Rong, M. Z.; Zhang, M. Q. Self-Healing Polymeric Materials based on Microencapsulated Healing Agents: From Design to Preparation. *Prog. Polym. Sci.* **2015**, *49*−*50*, 175−220.
(33) Guo, M. L.; Li, W.; Han, N.; Wang, J. P.; Su, J. F.; Li, J. J.; Zhang, X. X. Novel Dual-Component Microencapsulated Hydrophobic Amine and Microencapsulated Isocyanate Used for Self-Healing Anti-Corrosion Coating. *Polymers* **2018**, *10*, 319.
(34) Zhang, H.; Zhang, X.; Chen, Q.; Li, X.; Wang, P.; Yang, E.-H.; Duan, F.; Gong, X.; Zhang, Z.; Yang, J. Encapsulation of Shear Thickening Fluid as an Easy-to-Apply Impact-Resistant Material. *J. Mater. Chem. A* **2017**, *5*, 22472−22479.
(35) Salaün, F. Microencapsulation by Interfacial Polymerization. In *Encapsulation Nanotechnologies*; Mittal, V., Ed.; Scrivener Publishing LLC: Beverly, MA, 2013; Chapter 5, pp 137−174.
(36) Povey, A. C.; Nixon, J. R.; O'Neill, I. K. Membrane Formation and Characterization of Semi-Permeable Magnetic Polyhexamethyleneterephthalamide Microcapsules Containing Polyethyleneimine (PEI) for Trapping Carcinogens. *J. Microencapsulation* **1987**, *4*, 299−314.
(37) Perignon, C.; Ongmayeb, G.; Neufeld, R.; Frere, Y.; Poncelet, D. Microencapsulation by Interfacial Polymerisation: Membrane Formation and Structure. *J. Microencapsulation* **2015**, *32*, 1−15.
(38) Rang, M. J.; Miller, C. A. Spontaneous Emulsification of Oil Drops Containing Surfactants and Medium Chain Alcohols. *Prog. Colloid Polym. Sci.* **1998**, *109*, 101−117.
(39) Arshady, R. Preparation of Microspheres and Microcapsules by Interfacial Polycondensation Techniques. *J. Microencapsulation* **1989**, *6*, 13−28.

DOI: 10.1021/acs.jpcc.9b06544
J. Phys. Chem. C 2019, 123, 22413−22423